AIP | Applied Physics Letters

Improvement of near-infrared absorption linewidth in AlGaN/GaN superlattices by optimization of delta-doping location

C. Edmunds, L. Tang, J. Shao, D. Li, M. Cervantes et al.

Citation: Appl. Phys. Lett. **101**, 102104 (2012); doi: 10.1063/1.4751040
View online: http://dx.doi.org/10.1063/1.4751040
View Table of Contents: http://apl.aip.org/resource/1/APPLAB/v101/i10
Published by the American Institute of Physics.

Improvement of near-infrared absorption linewidth in AlGaN/GaN superlattices by optimization of delta-doping location

C. Edmunds,[1] L. Tang,[1,2] J. Shao,[1,2] D. Li,[1,2] M. Cervantes,[1] G. Gardner,[2,3] D. N. Zakharov,[2] M. J. Manfra,[1,2,3,4] and O. Malis[1,a)]
[1]*Department of Physics, Purdue University, West Lafayette, Indiana 47907, USA*
[2]*Birck Nanotechnology Center, West Lafayette, Indiana 47907, USA*
[3]*School of Materials Engineering, Purdue University, West Lafayette, Indiana 47907, USA*
[4]*School of Electrical and Computer Engineering, Purdue University, West Lafayette, Indiana 47907, USA*

(Received 30 July 2012; accepted 23 August 2012; published online 5 September 2012)

We report a systematic study of the near-infrared intersubband absorption in AlGaN/GaN superlattices grown by plasma-assisted molecular-beam epitaxy as a function of Si-doping profile with and without δ-doping. The transition energies are in agreement with theoretical calculations including many-body effects. A dramatic reduction of the intersubband absorption linewidth is observed when the δ-doping is placed at the end of the quantum well. This reduction is attributed to the improvement of interface roughness. The linewidth dependence on interface roughness is well reproduced by a model that considers the distribution of well widths measured with transmission electron microscopy. © *2012 American Institute of Physics*. [http://dx.doi.org/10.1063/1.4751040]

AlGaN/GaN superlattices have attracted interest for near- and far-infrared (1.3 to 143 μm)[1–6] intersubband (ISB) devices due to the large available conduction band offset (>1 eV), and longitudinal-optical phonon energy (~90 meV), respectively. These devices include light detectors and emitters tunable by design in broad spectral regions that are relatively inaccessible to other material systems. To measure near-infrared ISB transitions in nitrides, however, large charge densities ($>1\times10^{18}\,\mathrm{cm}^{-3}$) are typically required. These charge densities are achievable only through heavy Si doping. This Si doping has significant direct and indirect effects on important device parameters such as transition energy and linewidth that alter device performance. The strong influence of many-body effects such as depolarization shift and exchange interaction on ISB transition energies at high charge densities has already been investigated.[1,2,7] The effect of doping location on the ISB properties has also been explored, though no significant correlation was reported.[2,8] This paper focuses on the indirect effects of heavy Si doping on near-infrared absorption related to structural changes. We carried out a systematic study of the optical and structural properties of strained AlGaN/GaN superlattices grown on free-standing GaN substrates with various continuous and δ-doping schemes. δ-doping is an attractive technique to significantly increase charge density when the maximum bulk doping density is limited by the available Si source. We found a dramatic reduction of the intersubband absorption linewidth when using δ-doping at the end of the quantum wells (QWs) and we attribute it to improvement of interface roughness.

The AlGaN/GaN superlattices were grown by molecular beam epitaxy under Ga-rich conditions at 745 °C on low-defect c-plane free-standing GaN substrates from Kyma Technologies.[4–6] The substrates were un-intentionally doped for all but one sample that was semi-insulating. Nitrogen was supplied by a radio-frequency plasma source with a power of 300 W and a flow rate of 0.5 SCCM (SCCM denotes standard cubic centimeters per minute at STP). Silicon was provided as an n-type dopant by a high-purity solid-source filament cell. To determine the optimal doping scheme, several continuous and δ-doping profiles were considered. A summary of the doping schemes is given in Table I. The samples are structurally identical and differ only in the doping scheme. Moreover, the samples F-1 and F-2 are nominally identical in all respects (including doping scheme), and the experimental results are shown in Table I to illustrate the repeatability of the growth and absorption measurements. The 15-period AlGaN/GaN superlattices were characterized with high resolution transmission electron microscopy (HRTEM) and high-resolution x-ray diffraction (HRXRD). Theoretical simulation of the x-ray diffraction pattern using the commercial software package Panalytical X'PERT EPITAXY combined with HRTEM imaging allows for the determination of the well and barrier thicknesses as well as the Al composition. HRTEM images

TABLE I. Summary of the results for intersubband absorption measurements (transition energy and FWHM of dominant absorption peaks) for the samples investigated in this study. The location of the δ-doping is given in parenthesis in ML from the beginning of growth of the quantum well. W, well bulk doping; B, barrier bulk doping; and SI, sample grown on semi-insulating substrate. PIA indicates result of photo-induced absorption measurements.

Sample	Continuous doping	Delta doping position	Energy (meV)	FWHM (meV)
A	W	…	377 616 (PIA)	226 (PIA)
B	W + B	…	368 635	202 (PIA)
C	W + B, SI	…	436 688	177
D	W	W (10 ML)	675	94
E	W + B	W (10 ML)	654	98
F-1	W + B	W (3 ML)	672	220
F-2	W + B	W (3 ML)	709	224

a)Author to whom correspondence should be addressed. Electronic mail: omalis@purdue.edu.

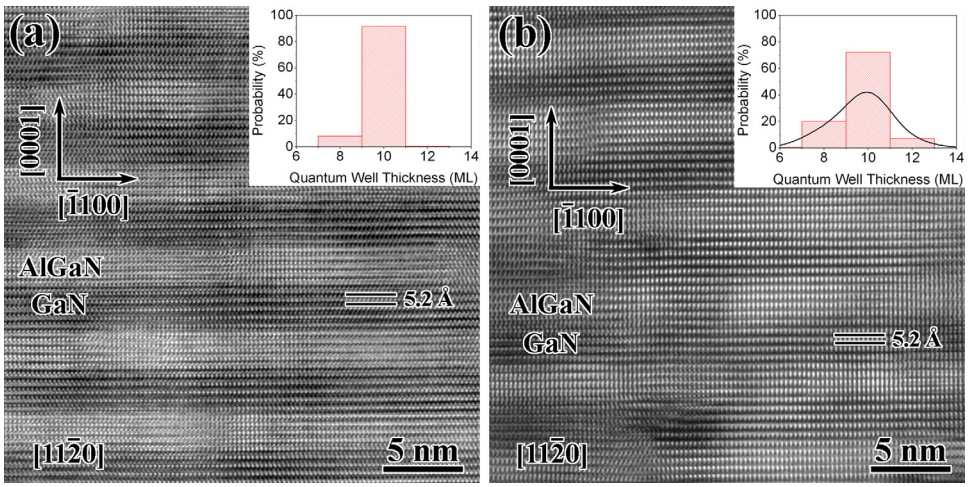

FIG. 1. HRTEM images of samples E (a) and F-1 (b), respectively. The GaN layer periodicity in the [0001] direction is 5.2 Å. Histograms represent the distribution of GaN quantum well widths obtained from image analysis. The solid black line denotes a continuous fit of the histogram in the inset of (b).

of samples E and F-1 (see Table I) are shown in Fig. 1. Based on measurements conducted on the HRTEM images, the samples were determined to contain on average 10 monolayer (ML) thick GaN QWs and 10 ML thick $Al_{0.70}Ga_{0.30}N$ barriers (1 ML is 2.6 Å thick). The capping layer consisted of an additional 10 ML thick $Al_{0.70}Ga_{0.30}N$ barrier. It should be noted that for the given TEM sample thickness, contrast on the HRTEM images reveals a 5.2 Å periodicity in the [0001] direction in the GaN layers. This periodicity corresponds to the GaN lattice unit cell that itself consists of 2 MLs. Thus, under the current imaging conditions, every other monolayer from the unit cell is visible. Consequently, this is limiting our layer thickness measurements to even numbers of MLs. Silicon doping levels were calibrated using secondary ion mass spectrometry. The bulk impurity density for GaN was measured to be $4 \times 10^{19}\,cm^{-3}$. To further increase charge density, δ-doping was applied in several samples during a growth pause of 5 min at the location indicated in Table I, i.e., either close to the middle of the QW (3 ML), or after the deposition of the QW (10 ML). During this pause, the Ga, Al, and plasma shutters were closed. The expected sheet charge density is $2 \times 10^{14}\,cm^{-2}$.

The optical properties of the samples were characterized using Fourier-transform infrared spectroscopy on samples polished into 45° multipass waveguides. Both direct and photoinduced absorption (PIA) measurements were carried out. In both measurements, a polarizer was used to isolate the ISB transitions. For PIA, an optically chopped 15 mW HeCd laser operating at 325 nm was used to modulate the well electron density and the infrared absorption was measured in step-scan mode using a lock-in amplifier. All absorption spectra are normalized to the number of the passes through the active region, coupling angle, and electric field overlap. The electric field overlap was estimated by calculating the average value of the electric field over the active region, assuming a node at the air-semiconductor interface.

The band structure of the AlGaN/GaN superlattices was calculated self-consistently using the eight-band k·p model with the nextnano[3] software.[9] The model includes screening of the polarization fields due to charge redistribution (self-consistent calculation). Photo-generated free-carrier screening was considered negligible because the optical pumping is done at relatively low-power and below the band-gap (in the near-infrared). A conduction band offset of 1.38 eV was assumed based on experimental measurements of the AlN/GaN valance band offset.[10] The many-body effects, including the exchange term, depolarization, and excitonic shifts, were estimated using the method described by Tchernycheva *et al.*[1,11–13] The material parameters used in the calculation are summarized in Ref. 14. The appropriate bowing parameters for AlGaN were used when available. Otherwise, a linear interpolation was assumed. The effects of these terms on the transition energy are summarized in Fig. 2.

Figure 3(a) displays the polarization-normalized ISB absorption spectra of the three samples without δ-doping (A, B, and C). Sample A is the most lightly doped sample in this study, i.e., bulk doped in the QW. The direct absorption spectrum of this sample is dominated by a peak at 375 meV (Fig. 3(a)), while the PIA spectrum is dominated by a peak at 590 meV (inset of Figure 3(a)). The low energy peak is attributed to transitions in the triangular well formed at the bulk-superlattice interface, while the high energy peak is attributed to the transition between the ground and the first excited state in the superlattice. The dominance of the

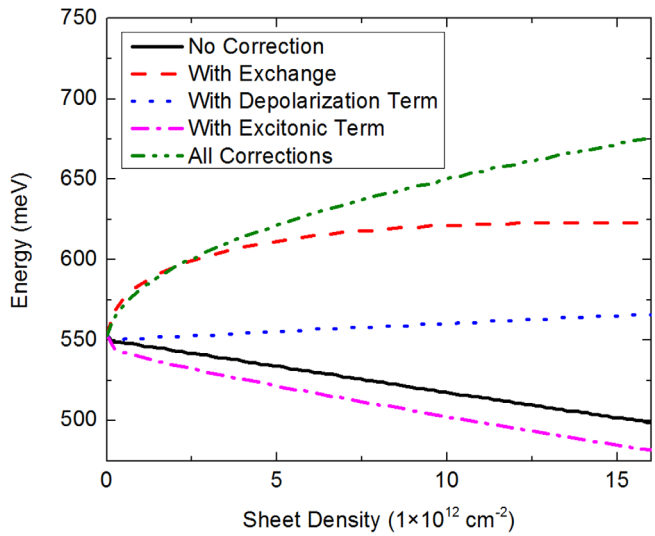

FIG. 2. Influence of the various many-body effects on the intersubband transition energy as a function of sheet charge density for a 2.6-nm QW with 2.6-nm barriers.

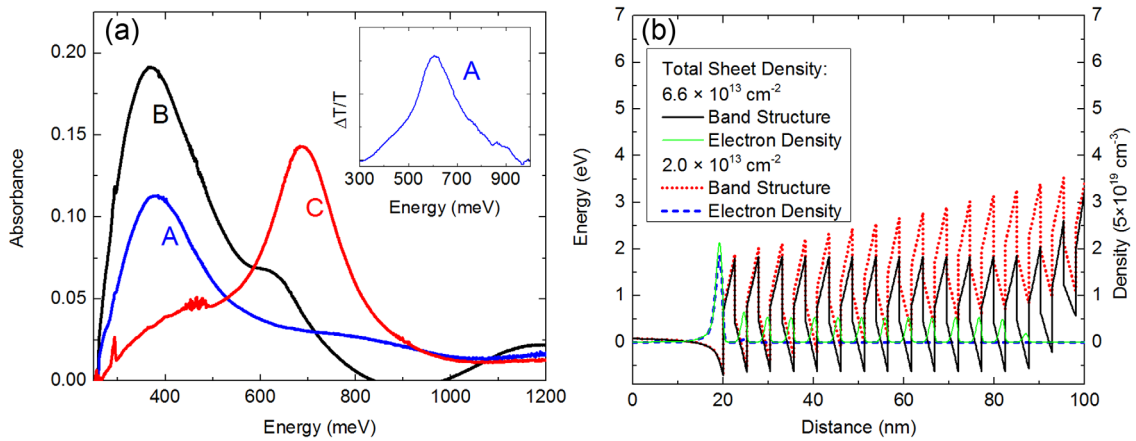

FIG. 3. (a) Absorbance spectra for samples A (blue), B (black), and C (red). Inset: PIA spectra for sample A. (b) Effect of Fermi-level pinning on the band structure and electron density distribution for two total charge densities. The superlattice surface is at 100-nm.

triangular well in the direct absorption spectrum can be explained by depletion of the superlattice due to Fermi-level pinning at the AlGaN cap layer under equilibrium conditions (Fig. 3(b)). The Fermi-level pinning in AlN has been estimated to be up to half the band gap.[15] In the PIA measurement, in contrast, additional charge is pumped in the structure from the valence band. This additional charge is likely to mainly fill the ground state of the superlattice and to produce the photoinduced signal at 590 meV. Since the PIA measurement is sensitive only to the modulated absorption, only the high energy peak is visible. The shift of the electron density from the triangular well to the superlattice with increasing charge density has been previously observed in electro-modulated absorption measurements.[16] Moreover, our peak assignment is supported by the spectrum of the slightly higher doped (bulk well and barrier doped) sample B (Fig. 3). For sample B, absorption peaks at both 368 and 635 meV are visible in direct absorption measurements (Fig. 3). The small increase in the superlattice transition energy of sample B with respect to sample A is also consistent with the increase in transition energy due to many-body effects (Fig. 2).

Sample C is nominally identical in structure to sample B but was grown on a semi-insulating substrate. In contrast to the previous two samples, the superlattice transition is dominant (Fig. 3). As discussed for sample B, the relative increase in the intensity of the superlattice transition is accompanied by an increase in transition energy, consistent with calculations of many-body effects (Fig. 2). To assess the accuracy of the many-body calculations, the total charge density for sample C was measured by Hall effect. A total sheet density of $2.29 \times 10^{14}\,\mathrm{cm}^{-2}$ was obtained, in agreement with the total sheet density of $2.49 \times 10^{14}\,\mathrm{cm}^{-2}$ calculated from band structure simulations based on the nominal doping level. Assuming this sheet density is split between the 15 QWs and the triangular well at the bulk-superlattice interface, the predicted charge density for a single QW is $1.6 \times 10^{13}\,\mathrm{cm}^{-2}$. At this sheet density, the calculated transition energy of 677 meV is in good agreement with the observed energy of 688 meV. Moreover, the calculated transition energy for the triangular well of 439 meV is also in agreement with the observed energy of 436 meV (charge density for the triangular well is $2.52 \times 10^{13}\,\mathrm{cm}^{-2}$). The quantitative difference between the nominally identical samples B and C can only be explained by the variability intrinsic to the MBE process (samples grown 6 month apart).

The absorbance curves for the delta doped samples are shown in Figure 4. Compared to the previous samples, the low energy transition is considerably weaker. This is consistent with the increased doping level. Moreover, the magnitude of the calculated absorbance was found to be in good agreement with experimental results (within $\sim$30%). The increased absorption observed in experiment is likely due to the spread of the δ-doping distribution into the barrier material, resulting in increased activation. The absorption lineshape shows a strong dependence on the δ-doping position. For the samples doped at the end of the well (D and E), a full width at half maximum (FWHM) of roughly 90 meV was obtained. This result is comparable to typical FWHM values reported in the literature for doped superlattices.[2] We emphasize that when the δ-doping was removed (samples A, B, and C) or placed closer towards the center of the well (samples F-1 and F-2), the FWHM increased to roughly 200 meV. The

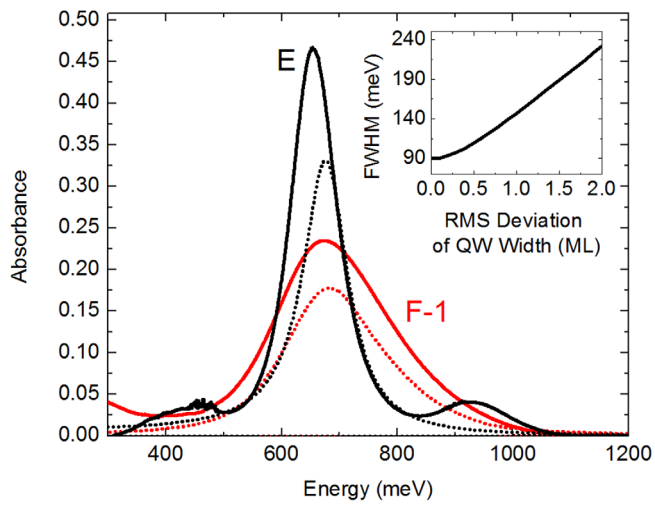

FIG. 4. Experimental (solid) and theoretical (dashed) absorbance spectra for samples E (black) and F-1 (red). Inset: Theoretical relationship between ISB linewidth and rms of the well-width distribution.

increase in FWHM is attributed to the difference in interface roughness observed in the HRTEM images of samples E and F-1 (Fig. 1).

To model the effect of interface roughness on broadening, the distribution of QW widths was determined from the HRTEM images in Fig. 1. The resulting width histograms are shown in the insets of Figure 1. In the case of sample E, roughly 91% of the quantum wells were 10 ML thick, within the accuracy provided by the image. Therefore, as expected, the contribution to the broadening due to interface roughness is minimal. For sample F-1, only 72% of the column thicknesses fell within 10 MLs. A continuous distribution of QW thicknesses was obtained by fitting the histogram with a smoothed series of Gaussians (Fig. 1(b) inset). The broadened absorbance spectrum was obtained by averaging the absorbance curves for various QW widths weighted by the distribution obtained from HRTEM analysis. In these calculations, a homogeneous broadening of 90 meV was assumed. The resulting curve is shown in Figure 4. The calculated FWHM for sample F-1 is roughly 200 meV, in close agreement with experimental results. Furthermore, the experimental absorbance curve for F-1 has a high energy tail that, according to our analysis, is due to the asymmetry of the QW width distribution towards narrower width. Given the qualitative and quantitative agreement between calculations and experiments, we believe valuable structural information can be derived from the absorption spectra. The inset of Fig. 4 shows the calculated dependence of the FWHM on the root-mean square (rms) of the QW width distribution and can be used to estimate the rms from experimental absorption measurements.

In summary, we have investigated the effect of doping profile on the near-infrared ISB absorption line profile of AlGaN/GaN superlattices. For low doping concentrations, the spectra are dominated by ISB transitions in the triangular well at the bulk-superlattice interface. As the doping concentration increased, the relative intensity of the quantum well transition increased. This trend was understood by accounting for the Fermi-level pinning at the surface. The accuracy of the many-body calculations was verified using Hall-effect measurements. Good quantitative agreement was obtained for the energy and magnitude of the intersubband transitions without modification of the material parameters obtained from the literature. In addition, the location of δ-doping in the structure was found to have significant impact on the intersubband absorption. The lowest FWHM (90 meV) was obtained when the δ-doping was located at the end of the well. This value is in agreement with typical values obtained in the literature for doped superlattices. Other doping schemes resulted in increased broadening up to 220 meV. The additional broadening was attributed to increased interface roughness and was accurately modeled by considering the distribution of quantum well thicknesses obtained from HRTEM analysis. The results indicate that δ-doping at the end of the well results in the best performance since the ISB absorption is enhanced while the linewidth is decreased. We emphasize that the improved lineshape is due to interface roughness improvement only, not to improved material quality. Material quality typically refers to material purity and the density of structural defects. We have no reason to believe that the δ-doping in the middle of the well leads to additional impurity incorporation. Moreover, the HRTEM indicates no additional structural defects in the sample δ-doped in the middle of the well. The improvement of the interface roughness may be due to the growth interruption at the GaN/AlGaN interface needed for Si-atom accumulation. During the 5 min pause, extra Ga atoms are consumed, leaving behind a smooth surface for AlGaN growth that overall improves the quality of the superlattice.

This work was supported by the NSF awards ECCS-1001431 and DMR-1206919 and from the Defense Advanced Research Project Agency (DARPA) under Contract No. D11PC20027.

[1]M. Tchernycheva, L. Nevou, L. Donyennette, F. H. Julien, E. Warde, F. Guilliot, E. Monroy, E. Bellet-Amalric, T. Remmele, and M. Albrecht, Phys. Rev. B **73**, 125347 (2006).
[2]P. K. Kandaswamy, F. Guillot, E. Bellet-Amalric, E. Monroy, L. Nevou, M. Tchernycheva, A. Michon, F. H. Julien, E. Baumann, F. R. Giogetta, D. Hofstetter, T. Remmele, M. Albrect, S. Birner, and L. S. Dang, J. Appl. Phys. **104**, 093501 (2008).
[3]H. Machhadani, Y. Kotsar, S. Sakr, M. Tchernycheva, R. Colombelli, J. Mageney, E. Bellet-Amalric, E. Sarigiannidou, E. Monroy, and F. H. Julien, Appl. Phys. Lett. **97**, 191101 (2010).
[4]D. Li, L. Tang, C. Edmunds, J. Shao, G. Gardner, M. J. Manfra, and O. Malis, Appl. Phys. Lett. **100**, 252105 (2012).
[5]C. Edmunds, L. Tang, D. Li, M. Cervantes, G. Gardner, T. Paskova, M. J. Manfra, and O. Malis, J. Electron. Mater. **41**, 881 (2012).
[6]O. Malis, C. Edmunds, M. J. Manfra, and D. L. Sivco, Appl. Phys. Lett. **94**, 161111 (2009).
[7]P. K. Kandaswamy, H. Machhadani, Y. Kotsar, S. Sakr, A. Das, M. Tchernycheva, L. Rapenne, E. Sarigiannidou, F. H. Julien, and E. Monroy, Appl. Phys. Lett. **96**, 141903 (2010).
[8]F. Guillot, B. Amstatt, E. Bellet-Amalric, E. Monroy, L. Nevou, L. Doyennette, F. H. Julien, and L. S. Dang, Superlattices Microstruct. **40**, 306–312 (2006).
[9]S. Birner, T. Zibold, T. Andlauer, T. Kubis, M. Sabathil, A. Trellakis, and P. Vogl, IEEE Trans. Electron Devices **54**, 2137 (2007).
[10]G. Martin, A. Botchkarev, A. Rockett, and H. Morkoç, Appl. Phys. Lett. **68**, 2541 (1996).
[11]K. M. S. V. Bandara, D. D. Coon, O. Byungsung, Y. F. Lin, and M. H. Francombe, Appl. Phys. Lett. **53**, 1931 (1988) [Erratum: **55**, 206(E) (1989)].
[12]S. J. Allen, Jr., D. C. Tsui, and B. Vinter, Solid State Commun. **20**, 425 (1976).
[13]W. L. Bloss, J. Appl. Phys. **66**, 3639 (1989).
[14]J. Wu, J. Appl. Phys. **106**, 011101 (2009).
[15]M. S. Miao, A. Janotti, and C. G. Van De Walle, Phys. Rev. B **80**, 155319 (2009).
[16]E. Baumann, F. R. Giorgetta, and D. Hofstetter, Appl. Phys. Lett. **89**, 101121 (2006).